ORDER, DISORDER, AND PHASE TRANSITION IN CONDENSED MEDIA

ANDREEV REFLECTION SPECTROSCOPY FeSe: ANALYSIS WITHIN THE FRAMEWORK OF A TWO-BAND MODEL

© 2024 V. A. Stepanov^{a,*}, M. V. Golubkov^a, A. V. Sadakov^a, A. S. Usoltsev^a, D. A. Chareev

^aLebedev Physical Institute of the Russian Academy of Sciences 119991, Moscow, Russia
^bKorzhinsky Institute of Experimental Mineralogy of the Russian Academy of Sciences 142432,
Chernogolovka, Moscow Region, Russia
^cDubna State University, 141982, Dubna, Moscow Region, Russia

d Institute of Physics and Technology, Ural Federal University 620002, Yekaterinburg, Russia
*e-mail: stepanov@lebedev.ru

Abstract. The Andreev reflection spectra $\sigma_{NS}(V,T) = dI/dV(V,T)$ of Ag/FeSe point contacts were measured in the temperature range T=4-14 K. Analysis of the spectra within the framework of a two-band model with order parameters of s-symmetry revealed two energy gaps Δ_i (i=1,2) and allowed us to plot their dependences on temperature. Approximation of the $\Delta_i(T)$ dependencies by a two-band isotropic model in the "pure" limit showed that their description requires taking into account both intraband and interband interactions of superconducting condensates. Such a description corresponds to s- or s^{++} -symmetry of the order parameter.

DOI: 10.31857/S004445102411e105

1. INTRODUCTION

The discovery of superconductivity in FeSe in FeSe 2008, the simplest layered iron-based superconductor, generated enormous interest that persists to the present day [1, 2]. Theoretical and experimental studies of the properties of this unusual superconductor are presented in numerous reviews, for example [2-5]. Let us note several important well-established properties of FeSe: 1) multi-band nature (two or even three bands) [6, 7]; 2) strong anisotropy of energy gaps [8–10]; 3) possibility of approximating measurement results using a twoband model with s-symmetry gaps [10–15]. The amplitudes of FeSe energy gaps and their momentum dependencies were measured using: 1) angleresolved photoemission spectroscopy (ARPES); 2) scanning tunneling microscopy (STM); 3) thermal conductivity measurements; 4) magnetic field penetration depth; 5) Andreev reflection spectroscopy [8–15]. Significantly fewer works are dedicated to measurements and, especially, analysis of energy gaps temperature dependencies $\Delta_i(T)$ (i = 1,2) within the multi-band model with determination of pairing interaction constants

$$\lambda_{ij}=V_{ij}N_j,\quad i,j=1,2,$$

where V_{ij} is the interaction strength, N_i is the density of states at the Fermi level [11, 15]. The multiband nature significantly complicates energy gap measurements. In single-band superconductors, $\Delta(T)$ can be measured directly from the position of conductance peaks in superconductor-insulatorsuperconductor (SIS) and superconductor-insulatornormal metal (SIN) tunnel junctions or normal metal-superconductor (NS) microcontacts in the Andreev reflection regime [16, 17]. In multi-band superconductors, conductances from different bands sum up, and to separate energy gaps Δ_i one has to use theoretical models that account for their number and symmetries [18–20]. This also applies to indirect methods of measuring energy gaps, where $\Delta_{i}(T)$ estimation is performed using gap-dependent characteristics, such as temperature dependencies of specific heat [10], magnetic field penetration depth $\lambda_{ab}^{-2}(T)$ [11], critical magnetic field $H_{c2}(T)$ [15].

Studies by the authors of work [11] on the depth of magnetic field penetration into FeSe crystals using μsR -spectroscopy revealed two energy gaps, $\Delta_1(0)=1.3$ meV and $\Delta_2(0)=0.5$ meV, with different critical temperatures $T_{c1,2}$ and dependencies $\Delta_{1,2}(T)$ of BCS (Bardeen-Cooper-Schrieffer) type in practically non-interacting bands. Measurements

of dependencies $\Delta_{1,2}(T)$ FeSe in work [12] using multiple Andreev reflections in break-junction contacts showed the presence of two energy gaps (without nodes): $\Delta_1(0) = 2.8 \text{ meV} (T_{c1} = 9.7 \text{ K})$ and $\Delta_2(0) = 0.8 \text{ meV} (T_{c2} = 6-7 \text{ K}), \text{ and dependencies}$ $\Delta_{1,2}(T)$ similar to those measured in work [11]. Measurements of Andreev reflection spectra of "soft" point contacts (PC) [18–20] Ag/FeSe (with conductive Ag paste as the non-superconducting electrode) conducted by the authors of works [13, 14] gave $\Delta_1(0) = 1.8$ meV and $\Delta_2(0) = 1.0$ meV with $T_{c1} = T_{c2}$ and dependencies $\Delta_{1,2}(T)$ close to BCS. Measurements in works [11-14] indicate practically complete absence or very weak interband interaction in FeSe. At the same time, study of temperature dependencies $H_{c2}(T)$ [15] in magnetic fields of different orientations with induction up to 38 T at temperatures up to $T/T_c \approx 0.3$ showed that the obtained results can be approximated by theoretical dependencies within the framework of a two-band isotropic model in the "clean" limit with predominant interband scattering.

In our work, Andreev reflection spectra $\sigma_{NS}(V, T)$ of stable soft PCs Ag/FeSe were studied in the temperature range. The aim of the work was to verify the applicability of the two-band model in the "clean" limit [21–24] with *s*-symmetries of energy gaps for analyzing temperature dependencies $\Delta_i(T)$ (i = 1,2) in FeSe, determining the constants of intraband and interband interactions, order parameter symmetry estimation.

2. EXPERIMENTAL METHODOLOGY

Several single-crystal FeSe plates with dimensions up to 1.2×0.7 mm² and thicknesses of 0.08-0.03 mm were used in the work, obtained by exfoliation of one relatively thick crystal. High-quality single crystals FeSe_{1-x} ($x \approx 0.04$) were grown from a melt solution of Fe powder and pieces of Se (Fe: Se = 1:0.94) in a mixture of AlCl₃: KCl = 2:1 in an evacuated to 10^{-4} bar and sealed quartz ampoule at a constant temperature gradient [25, 26]. Measurements of temperature dependencies of resistance with current along the plane ab of the crystal, $R_{ab}(T)$, and magnetic susceptibility $\chi(T)$ were conducted in home-made cryogenic inserts for a transport helium dewar at minimal currents and magnetic fields.

The description of methods for creating point contacts (PC), measuring their conductivity, and electronic components of the experimental setup

are provided in works [18–20, 27–29]. The classical method of creating PC is pressing a sharpened metal wire to another metal. In our work, Andreev reflection spectra – conductivity dependencies of ballistic $(d \ll l)$, where d is the contact diameter, l is the mean free path) microshorts (microcontacts) between superconducting FeSe and nonsuperconducting Ag on voltage, $\sigma_{NS}(V, T)$, were measured on soft PCs. PCs were created on the thin edge of the single crystal, which was cleaved immediately before applying a drop of conductive paste. The contact diameter did not exceed 0.1 mm. A ballistic microshort of Ag/FeSe PC should have a diameter of d < 120 nm and, accordingly, resistance of more than 5 Ohm [30]. Soft PCs consisted of multiple ballistic microshorts between Ag grains with sizes of $2-10 \mu m$ and the crystal [19, 31]. This allowed conducting spectroscopic measurements on contacts with resistance of 1-2 Ohm, as in works [13, 14]. The high stability of soft PCs made it possible to accurately measure conductivities $\sigma_{NS}(V, T)$ at different temperatures and the critical temperature of the contact T_c^A – temperature at which the characteristic structure associated with Andreev reflection disappears on the $\sigma_{NS}(V, T)$ dependence. The large difference in specific resistances along the plane ab and axis c FeSe ($\rho_c/\rho_{ab} \sim 500$ [36]) led to the fact that, despite the rough surface of the single crystal cleavage, the PC transport current always flowed along the ab plane of the sample.

Current-voltage characteristics (CVC) of contacts were recorded using a Keithley 2182A current source and 6221 multimeter. Conductances were obtained by numerical differentiation of CVC. The temperature was measured by a RuO-thermometer mounted on a copper base near the contact and stabilized by a heater with accuracy better than 0.01 K. Heater control was performed by a LabView program embedded in the temperature measurement subroutine. Conductances $\sigma_{NS}(V,T)$, measured at different temperatures, were normalized to the conductance in the normal state, $\sigma_N(V)$, measured at temperature, by several tenths of Kelvin higher than T_c^A . Normalized conductances

$$\sigma(V,T) = \sigma_{NS}(V,T)/\sigma_{N}(V)$$

were approximated by theoretical dependencies calculated using the two-band BTK (Blonder-Tinkham-Klapwijk) model with broadening parameters Γ (BTK- Γ) [18–20]. Fitting of calculated conductances to measured ones was performed

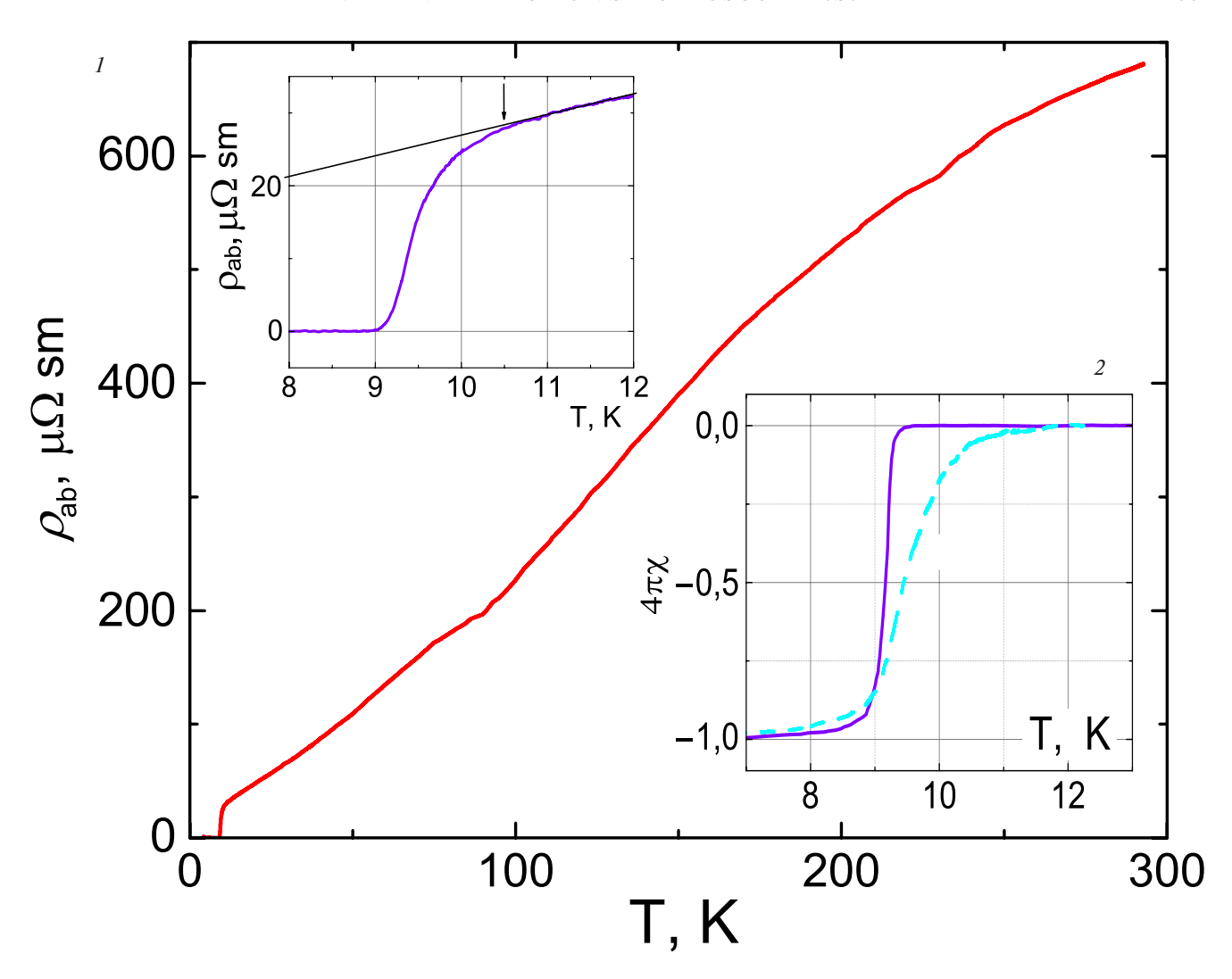


Fig. 1. Dependencies of specific resistance $\rho_{ab}(T)$ of one of the FeSe plates in the temperature range T = 4 - 300 K. At $T \approx 90$ K a feature related to the structural transition is visible. The insets show dependencies of $\rho_{ab}(T)$ and magnetic susceptibility $\chi(T)$ (curve 1) of the same sample near the superconducting transition temperature. The dashed line in the lower inset shows, in the same scale as dependence 1, the dependence $\chi(T)$ of FeSe crystal intercalated with organic solvents of conductive Ag-paste (curve 2). The shift of the beginning of the transition to the superconducting state towards higher temperature is clearly visible.

using the curvefit.m program from MatLab package based on the minimum sum of squares criterion for deviations between measured and calculated points. This made it possible to determine the values and temperature dependencies of FeSe energy gaps $\Delta_i(T)$ (i = 1, 2), contact characteristics $Z_i(T)$ (tunneling barrier strength parameter), $\Gamma_i(T)$ (broadening parameter) an wd (contribution of the first zone to the total contact conductance).

For approximation of temperature dependencies of energy gaps $\Delta_i(T)$ we used a simple model of two-band superconductor in the clean limit [21–24], which allowed qualitative determination of constants λ_{ij} of interband and intraband interactions of

condensates, energy gap amplitudes at T = 0 K and critical temperature T_c^{Δ} of the crystal at $\Delta_i(T_c^{\Delta}) = 0$.

3. MEASUREMENT RESULTS AND DISCUSSION

Figure 1 shows the dependencies of specific resistance $\rho_{ab}(T)$ and magnetic susceptibility $\chi(T)$ (curve 1) of one of the FeSe plates. They demonstrate typical features visible during crystal cooling [10, 32–35]. The critical temperature, width of transition to superconducting state, specific resistance, resistance ratio at 300 and 11 K are equal to $T_c = 9.3$ K, $\Delta T_c = 0.3$ K (according to magnetic susceptibility), $\rho(11 \text{ K}) \approx 28 \quad \mu\Omega \quad \text{cm}, \quad R(300 \text{K})/R(11 \text{ K}) = 23$

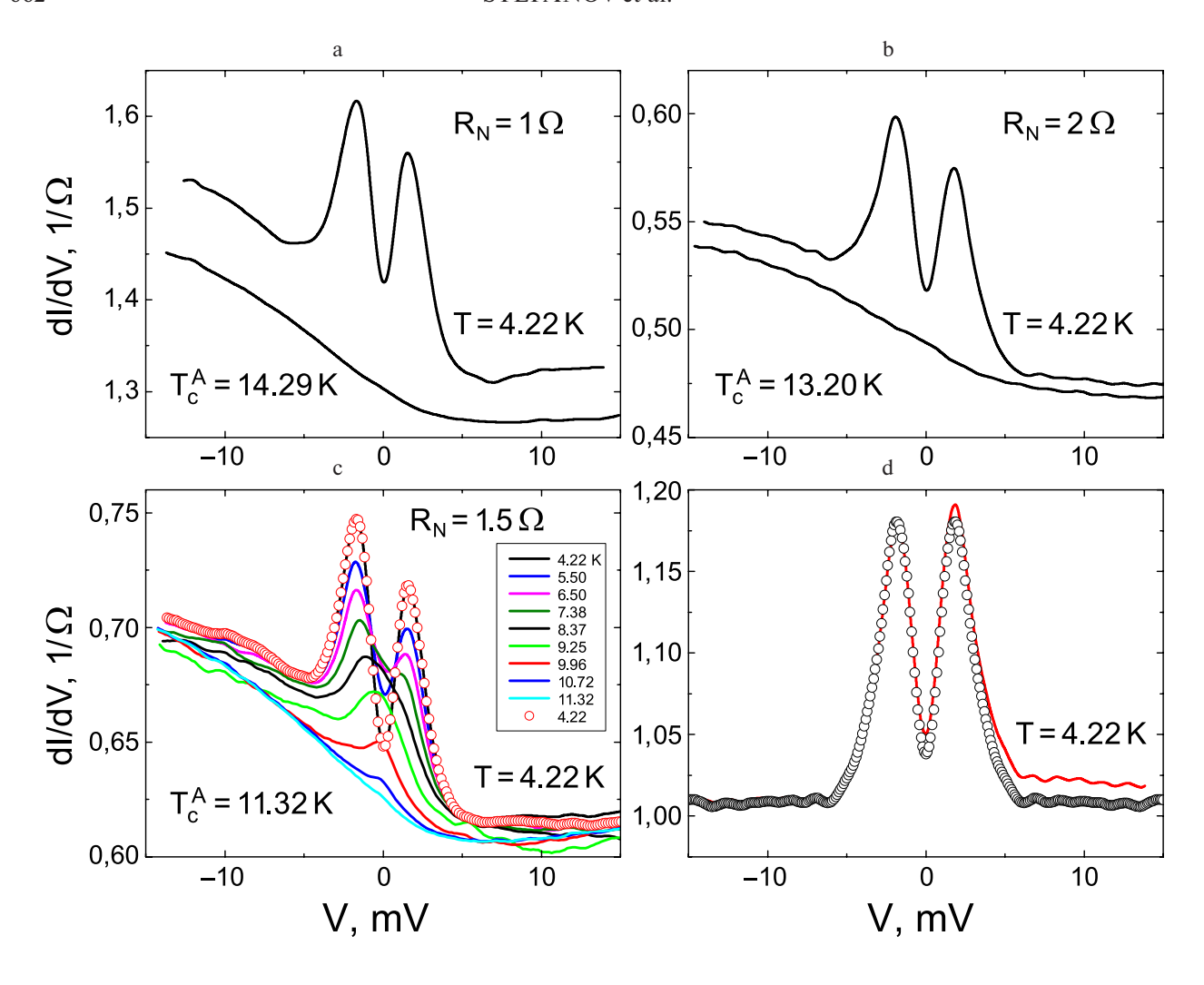


Fig. 2. Conductance recordings $\sigma_{NS}(V,T) = dI/dV$ of three soft PCs Ag/FeSe with resistances $R_N = 1(a)$, 1.5 (b),2 $(c)\Omega$ $(R_N = 0.5[R_N(-10 \text{ mB}) + R_N(+10 \text{ mB})])$ at T = 4.22 K and at the critical temperature of the Andreev contact T_c^A . Also shown are (b) recordings of several conductances at different temperatures. Contact stability is proven by the coincidence of conductances recorded at 4.2 K before temperature increase and after completion of temperature dependence recording. In Fig. d the red line shows the normalized conductance of PC (b) $\sigma(V, 4.22 \text{ K}) = \sigma_{NS}(V, 4.22 \text{ K})/\sigma_N(V, 11.3 \text{ K})$ and symbols show the symmetrized conductance of this contact. Small asymmetry, oscillations, and gap peaks persisted during normalization

respectively. These values are close to those measured in works [10, 32–36] and prove the high quality of samples.

PC was created between a drop of conductive paste (suspension of Ag microcrystals in a mixture of organic solvents [37]) and FeSe crystal. It is known that crystalline FeSe was easily intercalated by alkali metals and organic solvents. The critical temperature increased in this process [38]. Organic solvents of the conductive paste could change the sample surface properties in the drop area. To check the influence of conductive Ag-paste on FeSe, a small (approximately 0.1×0.2 mm²) crystal was placed in a drop of solvent for about 15 minutes (average time

from applying adhesive drop to the crystal during PC fabrication until its cooling). The magnetic susceptibility dependence of FeSe intercalated with adhesive solvent is shown in the lower inset to Fig. 1 by dashed line 2 alongside the dependence $\chi(T)$ of the main sample (curve 1). For ease of comparison, both dependencies are given in the same scale. It is evident that the Ag-paste solvent caused an increase in the width of the superconducting transition due to the rise in transition onset temperature by approximately 2 K. This proved that under the solvent action, a layer with higher critical temperature compared to the initial crystal forms on the FeSe surface. The transition onset temperature to the superconducting

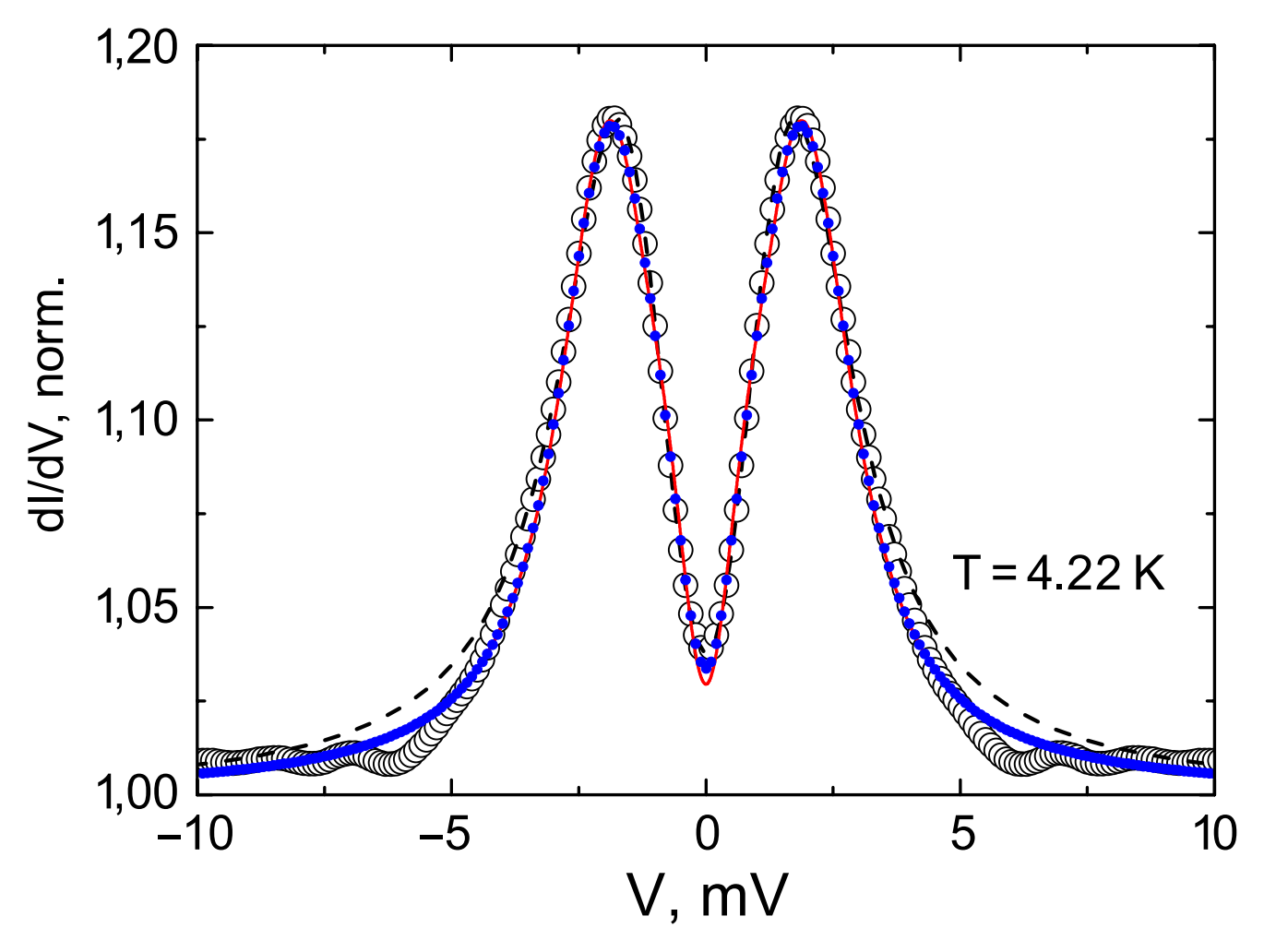


Fig. 3. Symbols – measured symmetrized conductance of the contact $\sigma(V, 4.22 \text{ K})$ (see Fig. 2*d*). Lines are approximations of the measured conductance. Dashed line is the approximation using single-band BTK-Γ model [17, 19] s(V, T, Δ, Γ, Z). Red line represents conductance calculated within the standard two-band model $\sigma(V, T) = \sigma_1(V, T, \Delta_1, \Gamma_1, Z_1)w + \sigma_2(V, T, \Delta_2, \Gamma_2, Z_2) \times (1 - w)$ [18–20]. Blue dots show conductance calculated using simplified two-band model [13, 14]

state of the intercalated layer reached 14.5 K for different samples.

In Figs. 2a, b, c the conductance records $\sigma_{NS}(V,T)$ of several PCs with resistances $R_N \approx 1$, 1.5, 2 Ohm at T = 4.22 K and $T_c^A \approx 11.3 - 14.3$ K are shown. Conductances recorded at T_c^A are the PC conductances in the normal state, $\sigma_N(V)$. Fig. 2b shows records of several PC conductances with resistance $R_N \approx 1.5$ Ohm at different temperatures. Contact stability is proven by the coincidence of conductances recorded at 4.22 K before temperature increase to T_c^A and after cooling the PC to the initial temperature. All features visible in the dependencies $\sigma_{NS}(V,T)$ PC were well reproduced. Conductances are asymmetric relative to point V = 0 mV. This feature $\sigma_{NS}(V,T)$ of soft PCs on FeSe was also noted in works [13, 14] and is apparently related to the semiconductor conductivity of the intercalated surface

layer FeSe [30, 39]. Similar asymmetry $\sigma_{NS}(V,T)$ was also observed during studies of doped (Li_{0.8}Fe₂)OH crystals FeSe ($T_c = 40 \text{ K}$) [40] using scanning tunneling microscope (STM). Dependencies $\sigma_{NS}(V,T)$ had a typical two-peak structure characteristic of Andreev reflection. Note that, as in other studies of Andreev reflection on FeSe, the measured conductances clearly show only peaks associated with the large gap Δ_1 at voltage $|V| = \Delta_1/e \approx 1.8 \text{ mV} [12-14]$. With temperature increase, the peaks converged and merged at $T \approx 8$ K. It can be seen that with increasing temperature, the contact conductances decreased by approximately 2% at T_c^A , significantly exceeding the critical temperature of FeSe (see Fig. 1). The increase of T_c^A to 13 K was observed when studying soft PC conductance in works [13, 14]. Obviously, the value of T_c^A of soft PCs reflected the critical temperature of the intercalated

FeSe surface layer, since at T > 10.5 K only this layer on the FeSe surface remained partially superconducting. The decrease in PC conductance with temperature increase could be related both to PC heating [19] and to the transition of part of the "sandwich" from intercalated FeSe layer and "pure" FeSe to normal state at T > 10.5 K. Discussion of this effect is provided at the end of this section. Similar dependencies $\sigma_{NS}(V,T)$ were obtained for all studied PC Ag/FeSe with resistances $R_N^{opt} = 0.7-2.5$ Ohm.

At PC resistances greater or less than, peaks at $|V| = \Delta_1/e$ on $\sigma_{NS}(V, T)$ were not resolved at $T \ge 4.22$ K. In Fig. 2d solid line shows normalized PC conductance $\sigma(V, T) = \sigma_{NS}(V, 4.22 \text{ K})/\sigma_N(V, 11.32 \text{ K})$. To eliminate asymmetry that interfered with approximation $\sigma(V, T)$, conductances were symmetrized as usual [8, 13, 14]. Symmetrized normalized PC conductance is shown in Fig. 2d by symbols. All features visible in dependency $\sigma_{NS}(V, T)$ were preserved during normalization and symmetrization.

Figure 3 shows the application of several theoretical models to approximate the measured conductance. Symbols represent measured at T = 4.22 K, normalized and symmetrized conductance $\sigma(V,$ 4.22 K) (see Fig. 2d). The lines show conductances approximating the measured one. The dashed line represents conductance $\sigma(V, T, \Delta, \Gamma, Z)$ calculated within the single-band BTK-Γ theory [17, 19] (3 free parameters), $\Delta = 1.54 \text{ meV} - \text{energy gap}$, $\Gamma = 0.57 \text{ meV} - \text{broadening parameter}, Z = 0.64$ tunnel barrier parameter. Parameter $\Gamma = \hbar/\tau$, where τ quasiparticle lifetime was introduced to account for the finite electron lifetime in metals of tunnel contact. Later this parameter was introduced into formulas describing Andreev reflection [19]. From a formal point of view, Γ includes all sources leading to broadening of dependence $\sigma(V,T)$: electron lifetime; electron scattering at the metal interface; energy gap anisotropy; thermal and electromagnetic noise. The value $Z = U_0/\hbar v_F$ in BTK theory determined tunnel barrier transparency (U_0 – barrier height, v_F – electron velocity at Fermi surface). The conductance of PC with a multiband superconductor electrode equals the sum of conductances into different bands. When using two-band model for calculating PC conductance, parameter w was introduced into dependence $\sigma(V,T)$, determining the contribution to conductance of the first band. In Fig. 3, the red line

shows conductance calculated using standard two-band model [18–20] (7 free parameters):

$$\sigma(V,T) = \sigma_1(V,T,\Delta_1,\Gamma_1,Z_1)w + \sigma_2(V,T,\Delta_2,\Gamma_2,Z_2)(1-w),$$

where σ_1 and σ_2 – Andreev contact conductances into first and second bands, $\Delta_1 = 2.04$ meV, $\Gamma_1 = 0.21$ meV, $Z_1 = 0.52$, $\Delta_2 = 0.21$ meV, $\Gamma_2 = 0$, $Z_2 = 1.7$, w = 041. Blue points – conductance calculated using simplified two-band model [13, 14] (5 free parameters), $\Delta_1 = 1.89$ meV, $\Delta_2 = 0.53$ meV, $\Gamma_1 = 0.18$ meV, $\Gamma_2 = 0.42$, $\Gamma_3 = 0.72$, $\Gamma_4 = 0.73$

It can be seen that in voltage range $|V| \le 3 \text{ mV}$ all three models described well the measured conductance $\sigma(V, 4.22 \text{ K})$. However, in a wider voltage range, two-band models described conductance significantly better. Conductances calculated using standard and simplified two-band models at T = 4.22 K are indistinguishable across the entire voltage range. Peaks corresponding to second energy gap $\Delta_2 \approx \pm 0.5$ mV [10] are broadened and were not resolved in measured dependencies, as in works by other authors [13, 14]. In absence of peaks associated with Δ_2 , seven free parameters in approximating dependencies $\sigma(V,T)$ led to unphysical growth of values $\Delta_{1,2}$ at T > 6 K. For this reason, we approximated measured conductances using simplified two-band model, as in works [13, 14].

The amplitudes of energy gaps Δ_1 and Δ_2 in FeSe as a function of temperature (T = 4.22 - 12 K), obtained by fitting conductances with a simplified two-band model, are shown in Fig. 4 by symbols. The temperature at which $\Delta_1(T) = 0$ ($T \approx 12$ K), was determined by the critical temperature of the intercalated surface layer of the FeSe crystal. In the range T = 4.2-9.5 K, the value $\Delta_1(T)$ changed smoothly, without sharp jumps. This indicated the absence of point contact heating with increasing temperature [41]. At T > 9.5 K, the sign of the curvature of the dependence $\Delta_1(T)$ changed to the opposite. The temperature dependence $\Delta_1(T)$ had a shape characteristic of a thin superconducting film on a superconductor with a critical temperature lower than that of the film [42]. This served as another confirmation of the presence of a thin intercalated layer on the crystal surface. The temperature at which the gap Δ_2 disappeared in the dependence $\sigma(V,T)$ was difficult to determine precisely due to its small magnitude and large broadening.

The inset to Fig. 4 shows the temperature dependencies of the fitting parameters Γ_1 (green

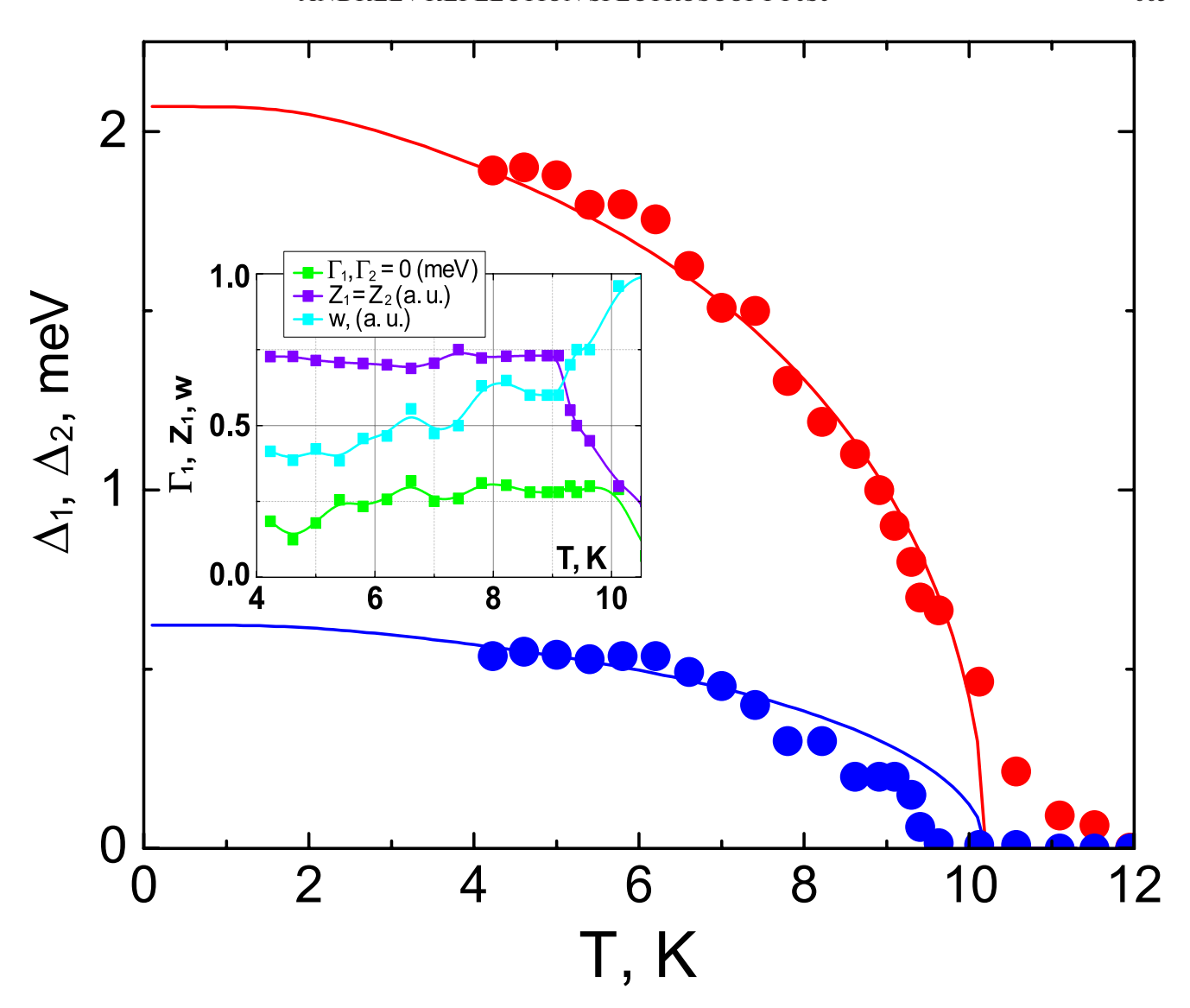


Fig. 4. Symbols – energy gaps Δ_1 and Δ_2 ($\Delta_1 > \Delta_2$) at different temperatures, obtained from approximating PC conductances (Fig. 3) with simplified two-band model. The inset shows temperature dependencies of approximation parameters Γ_1 , Z_1 , $w(\Gamma_2 = 0, Z_2 = Z_1)$. Lines – result of approximating dependencies $\Delta_1(T)$ and $\Delta_2(T)$ in temperature range 4.2–9.5 K with Moskalenko-Suhl two-band model (2) [21–24]

symbols), Z_1 (purple symbols), w (blue symbols). The arithmetic mean values of the parameters in the range T=4.2-9 K and their deviations from the mean are equal to $\Gamma_1=0.25\pm0.04$ meV, $Z_1=0.72\pm0.01$, $w=0.51\pm0.08$. The dimensionless parameter $Z_1(T)$ practically did not change with increasing temperature up to 9 K, as in work [13]. The broadening parameter $\Gamma_1(T)$, except for the temperature range 4-5 K, also did not strongly depend on temperature. Fluctuations of $\Gamma_1(T)$ and w in the range T=4-5 K could be caused by random noise. The parameter w, characterizing the contribution to the conductance of the first band point contact, had a relatively large temperature drift. The main reason for noticeable deviations of parameters Γ_1

and w from mean values was insufficient conditioning of the inverse problem in conductance calculations. At T > 9 K, the crystal began transitioning to the normal state (see Fig. 1), therefore the parameters Γ_1 , Z_1 , w began to change sharply with temperature.

Approximation of the measured dependencies $\Delta_{1,2}(T)$ in the temperature range 4.2–9.5 K was carried out using a simple two-zone Moskalenko-Zul model [21–24], taking into account the interaction of superconducting condensates of zones (λ^{00} -model with a minimal number of free parameters [23]):

$$\Delta_i = \sum_{j=1,2} \lambda_{ij} \Delta_j F(\Delta_j), \quad i = 1, 2, \tag{1}$$

where

$$\lambda_{ij} = V_{ij} N_j(0),$$

$$F(\Delta_i) = \int_0^{w_D} \frac{dE}{\sqrt{E^2 + \Delta_i^2}} \operatorname{th} \frac{\sqrt{E^2 + \Delta_i^2}}{2k_B T},$$

where E is energy, k_B is the Boltzmann constant, w_D is the characteristic energy of the phonon spectrum, for which the Debye energy is taken, $w_D = 13.67$ meV (in FeSe, the Debye temperature $T_D = 159$ K was measured in work [43]), or the energy at the end of the phonon spectrum 40 meV, measured in [44]. From equations (1) follow equations for calculating the temperature dependencies of energy gaps and the critical temperature of the sample T_c^{Δ} at the point where $\Delta(T_c^{\Delta}) = 0$:

$$\Delta_{1}(1 - \lambda_{11}F(\Delta_{1})) - \Delta_{2}\lambda_{12}F(\Delta_{2}) = 0,
\Delta_{2}(1 - \lambda_{22}F(\Delta_{2})) - \Delta_{1}\lambda_{21}F(\Delta_{1}) = 0.$$
(2)

We approximated the measured dependencies $\Delta_i(T)$ both with $w_D = 13.67$ meV and with $w_D = 40$ meV. Equations (2) were solved numerically. When selecting constants λ_{ij} for approximating the measured values $\Delta_1(T)$ and $\Delta_2(T)$ we aimed to minimize the sum of squares of deviations of measured points from calculated dependencies. The results of this work are shown in Fig. 4 by lines. The critical temperatures of zones 1 and 2 are equal. The critical temperature found at point $\Delta_i(T) = 0$ is $T_c^{\Delta} = 10.2$ K. This temperature coincided with the temperature of the crystal's transition onset to the superconducting state according to the dependence $\rho_{ab}(T)$ (see Fig. 1). The energy gaps of zones at T = 0 K are equal to

$$\Delta_1(0) = 2.09 \text{ meV}, \qquad \Delta_2(0) = 0.63 \text{ meV},$$

$$\Delta_1(0)/k_B T_c^{\Delta} = 4.7, \qquad \Delta_2(0)/k_B T_c^{\Delta} = 1.4.$$

The constants of intrazone and interzone interactions obtained during approximation: $\lambda_{11} = 0.63$, $\lambda_{22} = 0.13$, $\lambda_{12} = 0.7$, $\lambda_{21} = 0.09$. The energy gaps of zones at T = 0 K, $\Delta_i(0)$, taking into account the large anisotropy of FeSe energy gaps, are consistent with measurements made in other works.

The relatively large value of T_c^A (see Figs. 2a,b,c) was determined by the intercalated surface layer of the crystal, not by heating of the contact by transport current. This conclusion follows from measurement results which showed that 1) for all contacts, the

value of T_c^A is several degrees higher than the critical temperature of the FeSe crystal (see Figs. 2a,b,c) — when heated, it would be the opposite; 2) the energy gap Δ_1 (symbols) decreased smoothly with temperature rise, without sharp jumps (see Fig. 4) [41]. Measurement of magnetic susceptibility of intercalated FeSe showed that the surface layer of the sample began transitioning to the normal state at T > 8 K (see Fig. 1). In our PC, this led to an increase in resistance of the sandwich made of intercalated FeSe layer and pure FeSe with temperature in the range $T \approx 8-12$ K (see Fig. 2) and, consequently, to a decrease in contact conductance.

Let's evaluate the influence of the intercalated surface layer of FeSe on the dependencies we measured $\Delta_i(T)$. For this, let's consider the results obtained in work [42] when calculating temperature dependencies of energy gaps in films $Sn(T_c^{Sn} = 3.4 \text{ K})$ and $Al(T_c^{Al} = 1.2 \text{ K})$ in proximity contact using the McMillan model [45]. With weak coupling between the films in the density of states of the sandwich Sn-Al peaks from both Sn and Al energy gaps were present. The Al energy gap in the sandwich, $\Delta_{Sn-Al}(T)$, in the temperature range $T/T_c^{Al} = 0 - 0.9$ increased by 3–4% compared to the energy gap of pure Al, $\Delta_{Al}(T)$, and changed with temperature according to the BCS law. Only at $T/T_c^{\rm Al}=0.9-1.2$ the dependence $\Delta_{\rm Al}(T)$ noticeably deviated from the dependence for pure Al (see Fig. 2 in work [42]). We could not calculate the dependence $\Delta_1(T)$ for the intercalated FeSe layer, as we do not know its characteristics and cannot prove that the properties of the proximity structure "intercalated layer on the surface of FeSe-FeSe" satisfied the McMillan model [45]. Nevertheless, qualitatively, our measured normalized temperature dependence $\Delta_1(T)$ in the range $T/T_c^{\Delta} = 0.9 - 1.2$ coincided with that calculated in work [42] for weakly coupled Al and Sn films (Fig. 5). At $T/T_c^{\Delta} = 0 - 0.9$ the differences of our dependence $\Delta_1(T)$ from that calculated in work [42] are related to the deviation from BCS in two-band FeSe. Comparison of $\Delta_1(T)$ with the calculated dependence $\Delta_{AI}(T)$ in work [42] for the sandwich Sn-Al showed that due to small thickness and weak coupling with internal FeSe layers, the thin intercalated surface layer had minimal influence, no more than (3-4)%, on the amplitude Δ_1 and, consequently, on the form of dependence $\Delta_1(T)$ FeSe at $T \le 9.5$ K. The peak associated with the energy gap of the intercalated layer with relatively high temperature on the FeSe surface was not resolved in the measured conductances $\sigma_{NS}(V, T)$ due to large broadening related to the size and structure of soft PC

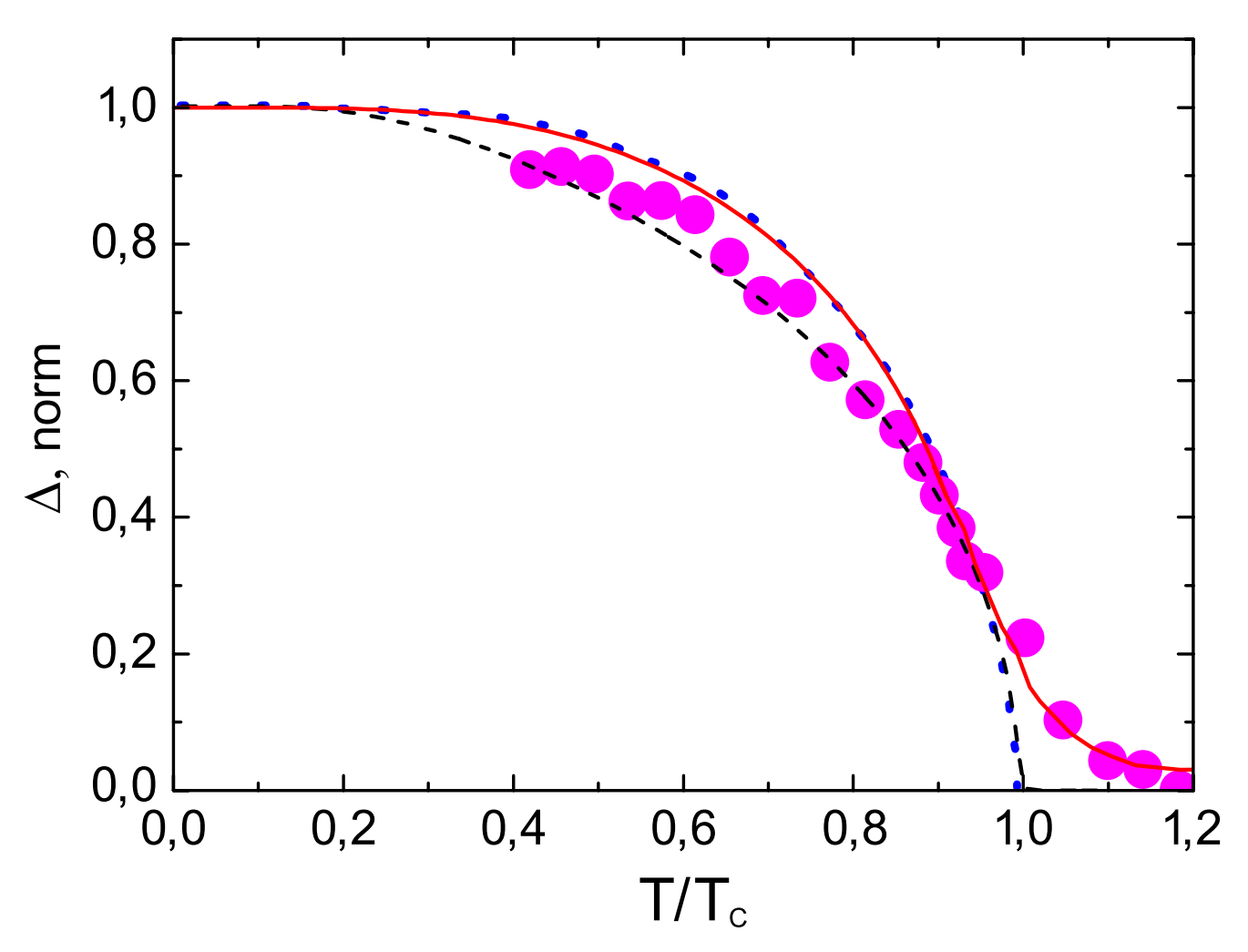


Fig. 5. Symbols and dashed line – measured and calculated from equations (2) temperature dependencies $\Delta_1(T)$ (Fig. 4) in normalized units $\Delta_1(T/T_c^{\Delta})/\Delta_1(0)$. Blue dots – normalized BCS dependence $\Delta_{A1}(T)/\Delta_{A1}(0)$. Solid red line calculated in work [42] normalized temperature dependence $\Delta_{A1}(T)/\Delta_{A1}(0)$ of the energy gap of Al for Sn and Al films in proximity contact

and inhomogeneity of this layer. Note that the energy gap dependence $\Delta_1(T)$, coinciding with $\Delta_{Al}(T)$ in the sandwich Sn–Al [42], can be easily obtained within the two-band model (2), assuming that FeSe and the intercalated layer on its surface are two different interacting superconductors.

The constants of intraband and interband interactions found during approximation of dependencies $\Delta_i(T)$ for energy $w_D = 13.67$ meV,

$$\lambda_{11} = 0.63$$
, $\lambda_{22} = 0.13$, $\lambda_{12} = 0.7$, $\lambda_{21} = 0.09$,

indicate relatively weak pairing in the first (strong) band and interband interaction comparable to the intraband one. The obtained values λ_{ij} are compatible with s- and s^{++} -symmetries of the order parameter. Despite the qualitative nature of the theory used for approximating dependencies $\Delta_{1,2}(T)$, the calculated

temperature dependencies of energy gap amplitudes and critical temperature of FeSe agree with the measured ones. When approximating the measured dependencies $\Delta_{1,2}(T)$ with calculated dependencies at $w_D = 40$ meV, only the values of λ_{ij} were changed. The conclusion about the role of intraband and interband interactions did not depend on the value of w_D . Approximation of measured dependencies in the absence of electron-phonon interaction in the weak band ($\lambda_{22} = 0$), with complete absence of interband interaction ($\lambda_{12} = \lambda_{21} = 0$) and with purely interband interaction ($\lambda_{11} = \lambda_{22} = 0$) of superconducting condensates proved impossible. Similar results were obtained for other soft PC.

The conducted studies do not agree with statements about the strength of interband scattering in works [11–14] and completely coincide with the conclusions of the authors of work [15]. Note that

the conclusions of works [13, 14] about the BCS-like dependence of band energy gaps $\Delta_{1,2}(T)$ when critical temperatures coincide $T_{c1} = T_{c2}$ contradict each other. At $T_{c1} = T_{c2}$ and $\Delta_1 \neq \Delta_2$ interband scattering λ_{12} must be finite and not very small. But at finite value λ_{12} dependencies $\Delta_{1,2}(T)$ should deviate from the BCS curve.

4. CONCLUSIONS

Using Andreev reflection spectroscopy, energy gaps of strong Δ_1 and weak Δ_2 bands of high- quality FeSe single crystals were measured in the temperature range 4.2–14 K. Analysis of dependencies $\Delta_{1,2}(T)$ within the framework of two-band λ^{00} -Moskalenko-Suhl model allowed determining the constants of intraband and interband interactions

$$\lambda_{11} = 0.63, \quad \lambda_{22} = 0.13, \quad \lambda_{12} = 0.7, \quad \lambda_{21} = 0.09,$$

energy gaps of bands at T = 0 K:

$$\Delta_1(0) = 2.09 \text{ meV}, \quad \Delta_2(0) = 0.63 \text{ meV}$$

and also calculate the critical temperature at which $\Delta_{1,2}(T) = 0$:

$$T_c^{\Delta} = 10.2 \text{ K}$$

The obtained results indicate weak pairing interaction in the first (strong) band, comparable interband interaction, and s- or s^{++} -symmetry of the order parameter.

FUNDING

The work of one of the authors (D. A. Ch.) was supported by UFU and IEM within the Strategic Academic Leadership Programs (PRIORITY-2030) and the state assignment of RAS FMUF-2022-0002.

ACKNOWLEDGMENTS

Authors V. A. S. and M. V. G. express sincere gratitude to the staff of Solid State Physics Department FIAN for their assistance in conducting this work.

REFERENCES

- 1. R. Liu, M.B. Stone, S. Gao et al., arXiv: 2401. 05092.
- **2.** *T. Shibauchi, T. Hanaguri, and Y. Matsuda*, J. Phys. Soc. Jpn. **89**, 102002 (2020).

- **3.** *S. Kasahara, Y. Sato, S. Licciardello et al.*, Phys. Rev. Lett. **124**, 107001 (2020).
- **4.** *G.R. Stewart*, Rev. Mod. Phys. **83**, 1589 (2011).
- **5.** *X. Liu, L. Zhao, S. He et al.*, J. Phys. Condens. Matter. **27**, 183201 (2015).
- **6.** *T. Terashima, N. Kikugawa, A. Kiswandhi et al.*, Phys. Rev. B **90**, 144517 (2014).
- 7. Y. Sun, S. Kittaka, S. Nakamura et al., Phys. Rev. B **96**, 220505 (2017).
- **8.** *D. Liu, C. Li, J. Huang et al.*, Phys. Rev. X **8**, 031033 (2018).
- **9.** P.O. Sprau, A. Kostin, A. Kreisel et al., Science **357**, 75 (2017).
- **10.** *L. Jiao, C.-L. Huang, S. Robler et al.*, Sci. Rep. 7, 44024 (2017).
- **11.** *R. Khasanov, M. Bendele, A. Amato et al.*, Phys. Rev. Lett. **104**, 087004 (2010).
- **12.** Ya.G. Ponomarev, S.A. Kuzmichev, T.E. Kuzmicheva et al., J. Supercond. Nov. Magn. **26**, 2867 (2013).
- **13.** Yu.G. Naidyuk, O.E. Kvitnitskaya, N.V. Gamayunova et al., Phys. Rev. B **96**, 094517 (2017).
- **14.** *D.L. Bashlakov, N.V. Gamayunova, L.V. Tyutrina et al.*, Low Temp. Phys. **45**, 1222 (2019).
- **15.** *M. Bristow, A. Gower, J. C.A. Prentice et al.*, Phys. Rev. B **108**, 184507 (2023).
- 16. I. Giaever, Phys. Rev. Lett. 5, 464 (1960).
- **17.** *G.E. Blonder, M. Tinkham, and T.M. Klapwijk*, Phys. Rev. B **25**, 4515 (1982).
- **18.** R.S. Gonnelli, D. Daghero, G.A. Ummarino, V.A. Stepanov et al., Phys. Rev. Lett. **89**, 247004 (2002).
- **19.** *D. Daghero and R.S. Gonnelli*, Supercond. Sci. Technol. **23**, 043001 (2010).
- **20.** *D. Daghero, M. Tortello, G.A. Ummarino, and R.S. Gonnelli*, Rep. Prog. Phys. **74**, 124509 (2011)
- **21.** *V. A. Moskalenko*, Fiz. Metal Metalloved. **8**, 503 (1959).
- **22.** *H. Suhl, B.T. Matthias, and L.R. Walker*, Phys. Rev. Lett. **3**, 552 (1959).
- **23.** *E.J. Nicol and J.P. Carbotte*, Phys. Rev. B **71**, 054501 (2005).
- **24.** A. Bussmann-Holder, arXiv: 0909.3603.
- **25.** *D. Chareev, E. Osadchii, T. Kuzmicheva et al.*, Cryst. Eng. Comm. **15**, 1989 (2013).
- **26.** *D.A. Chareev, O.S. Volkova, N.V. Geringer et al.*, Crystallogr. Rep. **61**, 682 (2016).
- **27.** *Yu.I. Gorina, M.V. Golubkov, T.I. Osina et al.*, Phys. Solid State **59**, 1918 (2017).
- **28.** S.I. Vedeneev, M.V. Golubkov, Yu.I. Gorina et al., JETP **154**, 844 (2018).
- **29.** V.A. Stepanov, M.V. Golubkov, JETP **157**, 245 (2020).
- **30.** Yu.G. Naidyuk, N.V. Gamayunova, O.E. Kvitnitskaya et al., Low Temp. Phys. **42**, 42 (2016).

- B 80, 060502 (2009).
- 32. S. Kasahara, T. Watashige, T. Hanaguri et al., Proc. Nat. Acad. Sci. USA 111, 16309 (2014).
- 33. J.K. Dong, T.Y. Guan, S.Y. Zhou et al., Phys. Rev. B 80, 024518 (2009).
- 34. S. Knoner, D. Zielke, S. Kohler et al., Phys. Rev. B 91, 174510 (2015).
- 35. A.E. Bohmer, V. Taufour, W.E. Straszheim et al., Phys. Rev. B 94, 024526 (2016).
- 36. A.A. Sinchenko, P.D. Grigoriev, A.P. Orlov et al., Phys. Rev. B 95, 165120 (2017).
- 37. RS PRO Silver Conductive Paint (in Google).

- 31. D. Daghero, M. Tortello, R.S. Gonnelli et al., Phys. Rev. 38. A. Krzton-Maziopa, V. Svitlyk, and E. Pomjakushina, J. Phys.: Condens. Matter 28, 293002 (2016).
 - 39. E. Venzmer, A. Kronenberg, and M. Jourdan, J. Supercond. Nov. Magn. 29, 897 (2016).
 - **40.** Y.J. Yan, W.H. Zhang, M.Q. Ren et al., Phys. Rev. B **94**, 134502 (2016).
 - **41.** D. Daghero, E. Piatti, N.D. Zhigadlo, and R.S. Gonnelli, Low Temp. Phys. 49, 886 (2023).
 - **42.** J. Vrba and S.B. Woods, Phys. Rev. B **4**, 87 (1971).
 - 43. G.A. Zvyagina, T.N. Gaydamak, K.R. Zhekov et al., arXiv: 1303.4948 (2013).
 - **44.** D. Phelan, J.N. Millican, E.L. Thomas et al., Phys. Rev. B 79, 014519 (2009).
 - 45. W.L. McMillan, Phys. Rev. 175, 537 (1968).